arXiv:2208.09565v1 [cond-mat.soft] 19 Aug 2022

Predicting Non-Equilibrium Folding Behavior of Polymer Chains using the Steepest-Entropy-Ascent Quantum Thermodynamic Framework

Jared McDonald,[1,*] Michael R. von Spakovsky,[2,†] and William T. Reynolds Jr.[1,‡]

[1] *Materials Science and Engineering Department, Virginia Tech, Blacksburg, VA 24061, USA*
[2] *Mechanical Engineering Department, Virginia Tech, Blacksburg, VA 24061, USA*

(Dated: 2021-08-22)

The Replica Exchange Wang Landau Method is used to estimate the energy landscape of a polymer composed of a simple hydrophobic and polar sequence using the HP protein model. Calculations of state transitions between the energy levels of the derived energy landscape are made using an equation of motion from the steepest-entropy-ascent quantum thermodynamic (SEAQT) framework. The SEAQT framework makes it possible to determine the unique kinetic paths from an arbitrary quasi-equilibrium or non-equilibrium initial state to stable equilibrium. Calculations performed with SEAQT require significantly reduced computational time versus comparable Monte Carlo simulations while providing otherwise unavailable thermodynamic and structural properties. SEAQT-derived kinetics are compared to experimentally derived intensity profiles describing the kinetics of the cytochrome-c protein using Rouse dynamic relations. Expected values for state averaged structural parameters are used to produce representative reconstructions of the calculated state-based evolution. Results show continuous transitions between states with no distinct folding phases. Changes in chain conformations during heating and cooling are more drastic along non-equilibrium paths than along quasi-equilibrium paths.

I. INTRODUCTION

Computational models of polymer folding have garnered considerable research interest over the last several decades. Molecular Dynamics and Monte Carlo models of polymer folding can provide information on the initial collapse of polymer chains and the formation of secondary and tertiary transient structures [1–3]. In recent years, advances in the entropic sampling of Monte Carlo-like systems have made thermodynamic descriptions of polymer systems easier to develop. An example is the non-Markovian Monte Carlo Wang-Landau algorithm [4, 5], which has improved thermodynamic analysis by allowing an estimate of the number of possible permutations of the occupiable states of the system,i.e., the degeneracy from only an energetic description of the system. Thus, the algorithm operates without regard to other non-thermodynamic information such as native contacts of the polymer chain or the reaction coordinates [1, 2, 6].

The ability to computationally estimate the energy landscapes of polymer systems has led to significant increases in an understanding of polymer folding for polymer chains of various lengths [4, 5], complex morphologies [7], and monomer site mutations [8]. It has also led to a clearer understanding of protein adsorption to surfaces [9] and has permitted doing simulations under varied environmental conditions [10–12]. Of particular interest in the studies of single polymer chains is the potential second-order phase transitions of the chain. These transitions typically include globular and coil transitions at high temperatures and a crystalline transition from the globular state at low temperatures. Polymer phase transitions are usually identified by changes in the heat capacity with temperature [4, 5, 13, 14]. However, utilizing the heat capacity to detect morphology transitions requires assuming the polymer's folding sequence will follow a continuous stable equilibrium path. This assumption is problematic for physical systems since the path is not at equilibrium but instead a non-equilibrium path and since, as others have stated, polymer folding is complex and the available transitional states vary greatly[15, 16].

Another problematic assumption is that phase transitions occur at local maxima in the heat capacity curve. However, this is not at all evident from a statistical analysis of the structural parameters of the chain. Chain conformations at evolving temperatures are commonly broader and occur slowly over large temperature changes. Thus, it can be difficult to qualitatively parse transitions.

In general, the exact kinetics of polymer folding is difficult to track as polymer relaxation times can occur over the length of milliseconds to a second. This is beyond the time scales of many atomistic models such as molecular dynamics[1, 2, 6]. On the other hand, Monte Carlo simulations can model folding kinetics to some extent [17–21] although these models have distinct disadvantages. Specifically, a system can become trapped in local equilibrium or metastable states. Additionally, Monte Carlo kinetics can be sensitive to the initial conditions, thus requiring that results be averaged over repeated runs for even small changes to a polymer's initial structure.

An alternative to these approaches, which is able to address all of these issues, is the steepest-entropy-ascent quantum thermodynamic (SEAQT) framework [22–47]. For a given system and given initial state, this framework is able to predict a thermodynamically unique kinetic path from any occupiable non-equilibrium state to stable equilibrium. It can utilize the same thermodynamic description provided by the Wang-Landau algorithm but does so without the statistical kinetic limitations inherent to a Monte Carlo model. Applying the principle of steepest entropy ascent, which has been suggested by

Beretta [48] as the fourth law of thermodynamics, the SEAQT equation of motion predicts the non-equilibrium state probability distribution at every instance of time along the kinetic path a system follows. This leads to a straightforward description of the energy and entropy evolution of a polymer system. Moreover, tracking the change in probability distribution makes it possible to calculate the non-equilibrium evolution of structural parameters such as the radius of gyration, tortuosity, and end-to-end distance [29]. The time evolution of such structural parameters provides an average physical representation of the chain at each point or state along the non-equilibrium kinetic path predicted by the equation of motion. These changes in properties do not have to follow a quasi-equilibrium path, so they can differ from those commonly studied in the literature.

It is the SEAQT framework and its application to predicting non-equilibrium polymer chain folding, that is presented here. The paper is organized as follows. Section II A describes the Hamiltonian used to represent the energy of a given polymer chain, and Section II B describes the Wang-Landau algorithm used to construct the energy landscape utilized by the SEAQT equation of motion. This is followed in Section II C by a description of this equation of motion. Section II D then provides an explanation of how the state space through which the SEAQT equation moves is linked to the kinetics of the polymer chain. Results for the application of the SEAQT framework to the evolution of two polymer chains are given in Section III followed by a discussion of these results in Section IV. The paper concludes with some final thoughts in Section V.

II. METHOD

A. Energy Landscape

We begin with a description of the Hamiltonian used in our model. The discrete energy levels, the E_j's, of the polymer system used to build the system's energy landscape are described by the HP (nonpolar-polar amino acid) model formulated by Dill *et al.* [49]. In this lattice model, the polymer chain is composed of amino acids with either hydrophobic or hydrophilic monomers. The chain energy is described as the sum of attractive interactions associated with the number of nearest-neighbor hydrophilic contacts. This energy, or Hamiltonian, is expressed as

$$E_j = \frac{1}{2}\sum_{n=1}^{N}\sum_{z=1}^{Z}\varepsilon_{n,z}^{\mathrm{HH}} \tag{1}$$

where $\varepsilon_{n,z}^{\mathrm{HH}}$ represents the interaction energy between two non-bonded adjacent hydrophobic monomers and is set to a value of -1. The summation is across the entire chain where N is the number of monomers in the chain and Z is the number of possible nearest-neighbor contacts for a monomer site on the lattice.

The polymer chain is modeled in a 3-dimensional cubic spin lattice with periodic boundary conditions, and the excluded volume effect is implemented as a self-avoiding walk [49]. The modeled monomers are simplified to only represent their hydrophilic or polar properties represented by the spin values of 1 and 2, respectively. In addition, the rotation angles of the lattice are limited to 90 degrees, and the bond length is a single lattice spacing. The linear size of the system is constrained to $N+2$ monomer bonds. This prevents the polymer from potentially interacting with itself through periodic boundary interactions.

The set of allowable movements along the polymer chain includes pull moves, reptation moves, rebridging moves, and pivot moves. The chosen distribution of movements is 75% pull and reptation moves, 23% bridging moves, and 2% pivot moves [4, 5, 50].

An accurate description of the system's energy spectrum enables all available conformations of the system to be distinguished and explicitly tracked to deduce the degeneracies, i.e., the density of states, of the system's energy landscape. The degeneracy is the number of distinguishable configurations that the system can take at a given energy, E_j. However, because of the enormous number of available conformations for a polymer chain, exact enumeration of the conformational space is limited to chains less than 30 monomers long [4, 51]. Thus, more advanced estimation techniques are required to derive the density of states for longer chains. One key method is the Wang-Landau algorithm [4, 5], which provides an *a priori* estimate of an energy landscape's degeneracy or density of states. This makes it possible to directly calculate the thermodynamic properties of the system including the expectation values of the energy and entropy once the probability distribution for energy level occupation is known.

B. Wang-Landau Algorithm

The Wang Landau algorithm uses entropic sampling of a discrete Monte Carlo-like system to estimate the system's density of states. This algorithm [52–54] is based on the principle that the probability of visiting the j^{th} energy level is $p_j = \frac{1}{g_j}$ where g_j is the degeneracy of the j^{th} energy level. The Wang Landau algorithm utilizes a stochastic method of moving through eigenstates with counters tracking the visits to a particular energy level the histogram and a counter for the density of states incremented by the modification factor, f dependent on the visited levels. Upon visiting an energy level, the histogram counter and density of states counter are both incremented by 1 and f respectively and the process is continued until the histogram is considered *flat* (that is, all the energy levels have been sampled uniformly). Flatness is achieved when the minimum histogram value is greater

than or equal to the average histogram value multiplied by the flatness criterion, which typically ranges between 80% and 100%. In this work, the flatness criterion is set to 99.2% based on accuracy and computational efficiency considerations. When the histogram is considered *flat*, the modification factor is halved and the stochastic sweep through eigenstates is repeated until f meets a threshold criterion [52–54], which is $f < 10^{-8}$ in this work.

Although the Wang Landau algorithm is applicable to any microcanonical ensemble, the characteristics of some physical systems slow the convergence of the method. In polymer systems, a very large number of energy levels, as well as a small number of difficult-to-reach levels, make it harder to estimate the density of states accurately. These problems are largely mitigated by the Replica Exchange Wang Landau algorithm, which parallelizes the Wang Landau algorithm. Replica Exchange Wang Landau divides the energy landscape into smaller energy ranges, or windows, with multiple Monte Carlo walkers moving independently in each energy window. To ensure convergence to the density of states for the whole energy landscape, the energy windows partially overlap each other, and information is shared periodically among walkers from different energy windows [52–55].

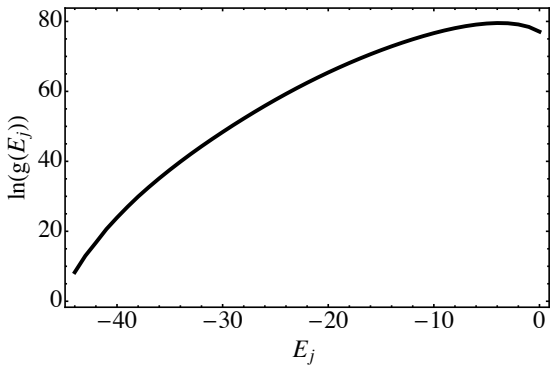


FIG. 1. The density of states represented by the natural log of the degeneracy of the j^{th} energy eigenlevel versus the energy, E_j, of each level. The density of states is for a 58-monomer polymer sequence calculated using Replica Exchange Wang Landau and a $60 \times 60 \times 60$ cubic lattice. The E_j are summed interaction energies of the hydrophobic-hydrophobic bounds.

Figures 1 and 2 show the estimated density of states and heat capacity curve for colorblack the 58-monomer chain modeled in this work, an amino acid sequence taken from Dill *et. al.* [16] . The move percentages used to generate the density of states for the energy landscape are those given in Section II A, and they were chosen by validating the density of states estimated with the Replica Exchange Wang Landau algorithm against the exact density of states for the 14 monomer chain studied by Bachmann *et al.* [51] .

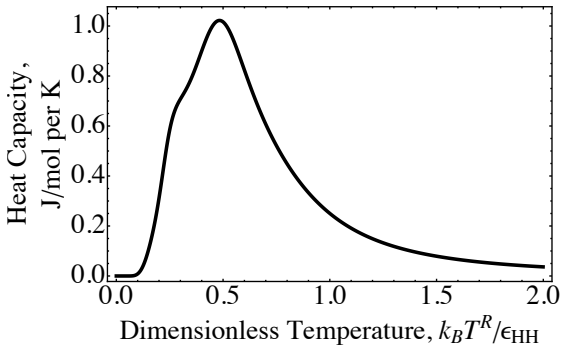


FIG. 2. The normalized heat capacity plotted versus temperature for the 58-monomer chain.

C. SEAQT Equation of Motion

The state of a polymer system is specified by the set of probabilities associated with the occupation of all the possible energy levels of the system. These occupation probabilities change with time as the system evolves from state to state. Using the system's energy landscape, i.e., its discrete energy spectrum and associated density of states, the equation of motion of the SEAQT framework predicts the unique time evolution of the probability distribution from an arbitrary non-equilibrium state to a stable equilibrium. It is, thus, able to predict the chain's morphological evolution solely on the basis of the principle of steepest entropy ascent. This principle reflects the redistribution of energy among available energy levels at every instant of time consistent with the laws of thermodynamics and mechanics.

Originally introduced and applied to small quantum systems in the 1970s and 1980s [42–47], the SEAQT framework has been extended over the past decade and a half to make it a practical tool for predicting non-equilibrium thermodynamic paths at all spatial and temporal scales. As a result, it has been applied to a multitude of chemical and material systems [22–39].

The SEAQT equation of motion for a simple quantum system [42] (or a model which mimics a quantum system such as an Ising or a Potts model) is expressed as:

$$\frac{d\hat{\rho}}{dt} = \frac{1}{i\hbar}[\hat{\rho}, \hat{H}] + \frac{1}{\tau(\hat{\rho})}\hat{D}(\hat{\rho}) \tag{2}$$

where $\hat{\rho}$ is the density operator, which represents the state of the system, and t is the time. If the system is classical, $\hat{\rho}$ becomes the set of occupation probabilities, p_j. The left-hand side and the first expression to the right of the equal constitute the von Neumann form of the time-dependent part of the Schrödinger equation of motion where $\hbar$ is the modified Planck constant and $\hat{H}$ is the Hamiltonian operator. The state evolution of that part of the equation is strictly reversible. The SEAQT

addition is given by the final term on the right, where $\hat{D}$ is the dissipation operator, which adds the nonlinear dynamics of irreversible state evolution absent in the von Neumann or Schrödinger equation, and τ is a relaxation parameter. This equation is valid for any irreversible process [22, 40, 41, 56] and although originally simply postulated by Beretta *et al.* [42], it subsequently has been derived via a variational principle along the direction of steepest entropy ascent by a constrained gradient descent in Hilbert space while preserving the energy and occupation probabilities [40].

The model of the polymer system used here, which contains multiple assumptions about the energetic interactions of the polymer system, the size of each monomer, and implicit bond considerations (Section II A), is strictly classical (no quantum correlations) and, thus, is treated as a quantum-inspired system using a Potts scheme. Because of this, $\hat{\rho}$ and $\hat{H}$ commute since they are diagonal in the energy eigenvalue basis [22–25, 41, 56]. For the case when the only generators of the motion, i.e., those operators which must be conserved, are the Hamiltonian and identity operator, the equation of motion can be expressed as

$$\frac{dp_j}{dt} = \frac{1}{\tau}\frac{\begin{vmatrix} -p_j \ln\frac{p_j}{g_j} & p_j & E_j\, p_j \\ \langle S\rangle & 1 & \langle E\rangle \\ \langle ES\rangle & \langle E\rangle & \langle E^2\rangle \end{vmatrix}}{\begin{vmatrix} 1 & \langle E\rangle \\ \langle E\rangle & \langle E^2\rangle \end{vmatrix}} \tag{3}$$

where

$$\begin{aligned} \langle E^2\rangle &= \sum_j p_j\, E_j^2 \\ \langle ES\rangle &= -\sum_j p_j\, E_j \ln\frac{p_j}{g_j} \end{aligned} \tag{4}$$

and p_j, E_j and g_j are the occupation probability, energy, and degeneracy, respectively, of the j^{th} energy eigenlevel. A quantity, $\langle\cdot\rangle$ represents the expectation value of a property such as the energy $\langle E\rangle$, entropy $\langle S\rangle$, and their product $\langle ES\rangle$. For entropy is defined utilizing the von Neumann form so that $S_j = -p_j \ln\frac{p_j}{g_j}$. This form is chosen as it is the only form which satisfies the characteristics required by the entropy of thermodynamics [57].

Equation (3) is only applicable to an isolated system although it can be extended to account for multiple subsystems interacting within a larger isolated system [22]. In this way, mass and heat transfer between sets of subsystems can be modeled. For example, Equation (3) can be modified to account for a heat interaction between two subsystems A and B so that the equation of motion of subsystem A becomes [22]

$$\frac{dp_j^A}{dt} = \frac{1}{\tau}\frac{\begin{vmatrix} -p_j^A \ln\frac{p_j^A}{g_j^A} & p_j^A & 0 & E_j^A p_j^A \\ \langle S^A\rangle & 1 & 0 & \langle E^A\rangle \\ \langle S^B\rangle & 0 & 1 & \langle E^B\rangle \\ \langle E\,S\rangle & \langle E^A\rangle & \langle E^B\rangle & \langle E^2\rangle \end{vmatrix}}{\begin{vmatrix} 1 & 0 & \langle E^A\rangle \\ 0 & 1 & \langle E^B\rangle \\ \langle E^A\rangle & \langle E^B\rangle & \langle E^2\rangle \end{vmatrix}} \tag{5}$$

Using the co-factors C_1, C_2^A, and C_3 determined from the first line of the determinate of the numerator and assuming the hypo-equilibrium condition developed by Li and von Spakovsky [22], the equation of motion for subsystem A reduces to the following form [22]:

$$\begin{aligned} \frac{dp_j^A}{dt^*} &= p_j^A\left(-\ln\frac{p_j^A}{g_j^A} - \frac{C_2^A}{C_1} - E_j^A\frac{C_3}{C_1}\right) \\ &= p_j\left[(S_j^A - \langle S^A\rangle) - (E_j^A - \langle E^A\rangle)\frac{C_3}{C_1}\right] \end{aligned} \tag{6}$$

with the variables t and τ replaced by a dimensionless time defined as $t^* = \int_0^t \frac{1}{\tau(\vec{p}(t'))}dt'$. The relaxation parameter, τ, can either be assumed constant or taken to be a function of the time-dependent occupation probabilities p_j represented by the vector $\vec{p}$. In what follows, τ is assumed to be a constant that scales the dimensionless time, t^* to actual time. The equation for subsystem B is written in a similar fashion. However, if subsystem B represents a temperature reservoir, its state does not change in time so that its equation of motion is not needed and the co-factor ratio in Equation (6) reduces to a function of the temperature of the reservoir, T^R, such that [22, 23]

$$\beta^R = C_3/C_1 = \frac{1}{k_b T^R} \tag{7}$$

The initial condition or state for the system of equations in Equation (6) is given by a distribution of occupied energy levels. For example, to generate initial conditions far from equilibrium for the 58-monomer system shown in Figure 2, Each the initial distribution is found by solving a system of equations comprised of a partially canonical distribution and the energy of the system after which the distribution is perturbed to a non-equilibrium distribution. The formulation of the partially canonical distribution is given by

$$p_j^{pe} = \frac{\delta_j\, g_j \exp(-\beta^{\rm pe} E_j)}{\sum_j \delta_j\, g_j \exp(-\beta^{\rm pe} E_j)} \tag{8}$$

where each δ_j can have a value of 1 or 0, depending upon whether or not the j^{th} energy eigenlevel is occupied. Each set of δ_j values leads to a particular partially canonical distribution since multiple partially canonical states exist for each value of the system energy, $\langle E\rangle$. Moreover,

β^{pe} is a parameter value unique to each partially canonical state and is inversely proportional to the temperature when the state is fully canonical.

D. Linking State Space to Chain Conformations

Previous applications of Monte Carlo methods to polymer chains provide quasi-equilibrium properties [4, 55, 58]. The SEAQT equation of motion allows one to predict changes in these properties along any thermodynamic path and, in particular, along non-equilibrium paths.

The solution to the SEAQT equation of motion predicts time-evolution through thermodynamic state space and does so without any *a priori* assumption about the underlying kinetic mechanism(s). This contrasts with other deterministic and stochastic modeling techniques in which a kinetic mechanism must be assumed. The predictions made by the SEAQT equation of motion are, thus, driven exclusively by the steepest entropy ascent principle, which captures the energy transitions between energy eigenlevels, and as a result, the behavior of the phenomena present. It does this at a fraction of the computational overhead of mechanistic approaches. In addition, when the energy landscape is topographically rough, there is no danger of the system becoming trapped in a metastable state (i.e., a partially canonical state) [2, 29] because it is the expectation values of the system energy and entropy that are tracked through state space, and the global stability criterion used to construct the equation of motion requires that only at stable equilibrium — i.e., when the state is canonical — are all the eigenlevels occupied and the time derivatives of all the associated probabilities zero.

Nevertheless, in order to describe changes in chain conformations or changes in specific physical properties with time, it is necessary to consider more than simply the energy and entropy state variables. There is an enormous number of chain conformations at each point of state space, so establishing how any particular chain evolves in time requires selecting the physically related conformations along the path in state space from among many different possibilities. This can be done with microstructural descriptors that link related chain conformations through a procedure described in detail in Reference [29]. The descriptors used here are parameters associated with the chain conformation: namely, the radius of gyration (R_g), the tortuosity (τ), and the end-to-end distance (R_E) of the polymer chain [4, 55, 58]. By requiring that one or more descriptors vary smoothly along the state path, conformations or properties in the physical system will also evolve smoothly with time.

The radius of gyration is calculated via the expression:

$$R_g = \left(\frac{1}{N} \sum_{i}^{N} \|\boldsymbol{r}_i - \boldsymbol{r}_{\rm cm}\|^2 \right)^{\frac{1}{2}} \tag{9}$$

where N is the number of monomers in the system, $\boldsymbol{r}_i$ is the 3-dimensional location vector of a given monomer, and $\boldsymbol{r}_{\rm cm}$ is the calculated location of the center of mass of the chain. Note that all simulated monomers are assumed to have the same mass. The radius of gyration provides a quantitative assessment of the distribution of mass of the polymer chain.

The tortuosity employed here is:

$$\tau = \left(\frac{1}{N-2} \sum_{i}^{N-2} \|\boldsymbol{s}_i - \bar{\boldsymbol{s}}\|^2 \right)^{\frac{1}{2}} \tag{10}$$

where $\boldsymbol{s}_i$ is a local vector at the $i-$th -mer that reflects the cumulative turns along the chain and $\bar{\boldsymbol{s}}$ is the mean of these vectors. The vector $\boldsymbol{s}_i$ has components:

$$\boldsymbol{s}_i = \begin{pmatrix} \sum_{j=1}^{i} w_{j_x} \\ \sum_{j=1}^{i} w_{j_y} \\ \sum_{j=1}^{i} w_{j_z} \end{pmatrix}$$

with the "turn vector," $\boldsymbol{w}_j$, defined by,

$$\boldsymbol{w}_j = \boldsymbol{r}_{j,j+1} \times \boldsymbol{r}_{j,j+2}, \qquad 1 \le i \le (N-2)$$

To calculate $\boldsymbol{s}_i$, the cross product of vectors from the current monomer to the next two monomers in the sequence (i.e., $\boldsymbol{r}_{j,j+1} = \boldsymbol{r}_{j+1} - \boldsymbol{r}_j$ and $\boldsymbol{r}_{j,j+2} = \boldsymbol{r}_{j+2} - \boldsymbol{r}_j$) are determined and their x, y, and z components summed. Whenever the polymer chain bends, it produces a non-zero $\boldsymbol{w}_j$ that is oriented perpendicular to the plane of the turn. The tortuosity is determined from the difference between the cumulative mean turns along the entire length of the chain, and it represents a measure proportional to the number of turns present along the chain segments. It is zero for a straight chain.

The end-to-end distance, R_E, given by

$$\begin{aligned} R_E &= \|\boldsymbol{r_0} - \boldsymbol{r_N}\| \\ &= \sqrt{(x_0 - x_N)^2 + (y_0 - y_N)^2 + (z_0 - z_N)^2} \end{aligned} \tag{11}$$

is the distance between the head of the chain, with coordinates $\boldsymbol{r_0} = \{x_0, y_0, z_0\}$ and the tail of the chain, $\boldsymbol{r_N} = \{x_N, y_N, z_N\}$.

A direct link between state space and chain conformations would involve associating the structural parameters with conformations in each energy level, but this approach is impractical because the degeneracy of each E_j is far too large to record even a small fraction of the chain conformations [29, 51]. Instead, a strategy is employed to identify and record only those conformations that lie along the kinetic path. First, at each energy level sampled by the Replica Exchange Wang Landau algorithm, the arithmetic average is found for descriptors R_g, τ, and R_E. Next, the SEAQT equation of motion is solved for the occupation probabilities of the energy eigenlevels along the kinetic path. Once these predicted probabilities are known, they are multiplied by the arithmetic averages at each energy level to obtain the expectation values of the structural parameters along the kinetic

path. Finally, to determine representative chain conformations along the path, the Replica Exchange Wang Landau algorithm is run a second time to record specific conformations. During this second Monte Carlo walk, conformations are recorded only for occupied energy levels with descriptor values close to the expected values obtained from the SEAQT equation of motion. Since the occupied energy levels are much fewer than the allowable levels and the expected descriptor values eliminate all but a few of the degenerate conformations, the procedure yields a small set of conformations that evolve smoothly with time along the kinetic path.

Scaling the rate with which the simulated system traverses the kinetic path to real-time can be accomplished by linking τ to physical quantities like a diffusion coefficient or other experimental data. How this is done is outlined in Section IV.

III. RESULTS

The evolution of a 58-monomer chain is tracked for two types of thermal interactions: an exchange of heat with a low-temperature reservoir, and an exchange of heat with a high-temperature reservoir. For each of these interactions, two kinetic paths are considered: (1) a path that starts at a non-equilibrium initial state and ends at equilibrium with the reservoir, and (2) a quasi-equilibrium path that starts at an initial state whose temperature is different from the reservoir's and moves through equilibrium states until it reaches the reservoir temperature. The same initial non-equilibrium state and initial quasi-equilibrium state are employed for both types of thermal interactions. The SEAQT equation of motion solution, which is a system of first-order ordinary differential equations in time, is solved using Matlab's ODE45 differential equation solver.

A. Interactions with a Low-T Reservoir

The quasi-equilibrium and non-equilibrium kinetic paths during a thermal exchange with a low-temperature reservoir are represented as parametric curves on the entropy–energy diagram of Figure 3. The black curve represents equilibrium (canonical) states; the tangent to this curve at any point is the temperature. The solid red curve is the quasi-equilibrium path and the dashed gray curve is the non-equilibrium path predicted by the SEAQT equation of motion. For both curves, the solid black points represent successive times along the path from the initial state to the final equilibrium state associated with the reservoir temperature, $T_{\rm R}$. The non-equilibrium path (dashed gray) and the quasi-equilibrium path (solid red) show the energy and entropy decreasing as heat is extracted from the polymer and flows into the reservoir. The system moves towards mutual stable equilibrium with the low-temperature reservoir, which is

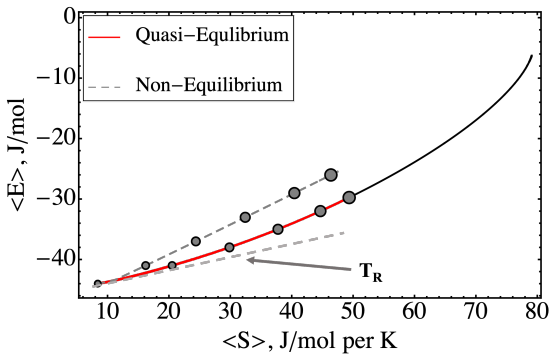


FIG. 3. The SEAQT predicted non-equilibrium path (dashed gray curve) and quasi-equilibrium path (solid red curve) associated with the 58-monomer chain system interacting with a low-temperature reservoir. The dashed light gray line denotes the tangent to the curve of stable equilibrium states (black curve) and is equal to the reservoir temperature. The paths are marked with circles to represent the energy and entropy of the polymer chain conformations shown in Figure 5. The largest circles are the initial states of the two paths, the smallest circle is the final stable equilibrium state at the reservoir temperature.

at a non-dimensional temperature $k_b T^R/\varepsilon^{\rm HH} = 0.125$ K where $\varepsilon^{\rm HH}$ is the negative of the interaction energy in Equation (1). The two paths through state space indicate the difference between an *idealized* quasi-equilibrium path and a *real* non-equilibrium path during the cooling. Next, we explore how the parameters associated with the chain conformation evolve along these two kinetic paths.

The time evolution of the descriptors R_g, τ, and R_E are shown in Figure 4. The expectation values for the radius of gyration nearly overlap during quasi-equilibrium cooling and non-equilibrium cooling. Although the curves are similar, the initial value for the non-equilibrium curve is significantly larger, indicating a less defined core and thus a wider distribution of mass from the growing hydrophobic core versus that at stable equilibrium. The expectation value for R_g along both paths decreases rapidly from the respective initial states to the stable equilibrium value at the reservoir temperature.

For the tortuosity descriptor, there is an initial rapid increase in τ during non-equilibrium cooling followed by a more gradual change to the final equilibrium value. That more moderate change is also experienced by the quasi-equilibrium path, although the curve begins with an amount of system folding closer to that of the final stable equilibrium state. Note that the initial inflections in the quasi-equilibrium curve at the beginning of the evolution are not physical but it is instead an artifact of the coarseness of the limited bond angles associated with the cubic lattice ($60\times60\times60$) used here and of the limited number of conformations (i.e., low degeneracies) associated with the lowest energy eigenlevels. The latter are in

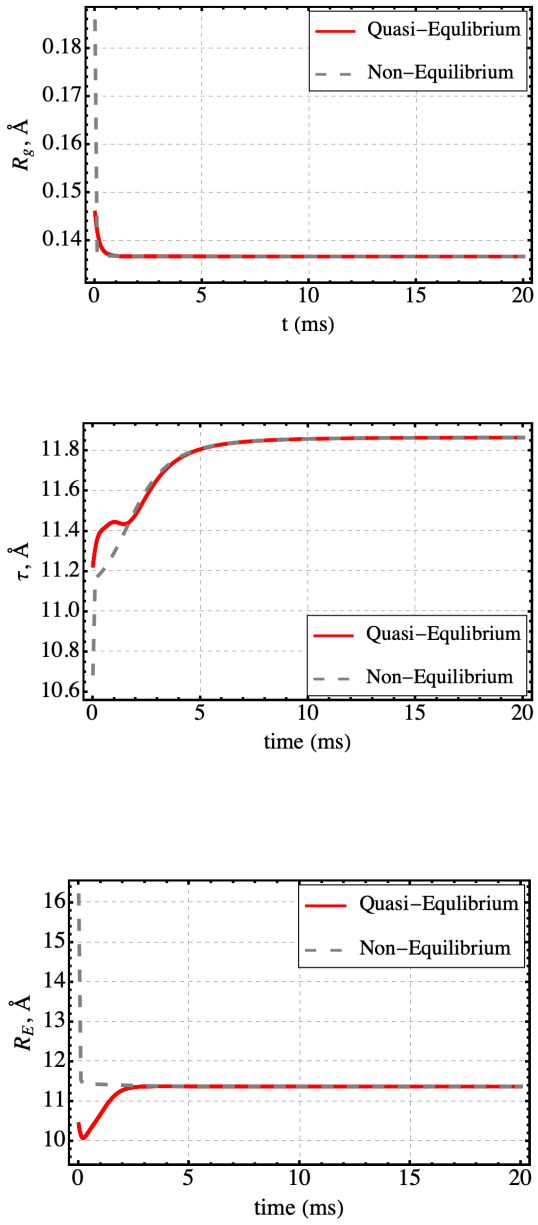


FIG. 4. Evolution of the expectation values of the radius of gyration, R_g, the tortuosity, τ, and the end-to-end distance, R_E, for both the quasi-equilibrium and non-equilibrium paths as the polymer chain interacts with a low-temperature reservoir.

play because of the interaction of the polymer chain with the low-temperature reservoir. As will be seen below, this problem does not appear with the polymer chain interacting with the high-temperature reservoir because the lower energy eigenlevels play no significant role at higher temperatures.

Like tortuosity, R_E initially differs along the non-equilibrium and quasi-equilibrium cooling paths. The end-to-end distance starts high for the non-equilibrium path and sharply decreases, while for the quasi-equilibrium path, the initial value is lower, experiences a slight decrease, then gradually increases. Note that the initial decrease is not necessarily physical but is instead an artifact for the same reason given for the initial inflection in the quasi-equilibrium τ curve. For both R_E paths, there is little change after about 3 ms at which time the value corresponding to the stable equilibrium state with the low-temperature reservoir is reached.

The expected chain conformations along the non-equilibrium and quasi-equilibrium paths of Figure 3 are shown in Figure 5. The upper row of images represents six instances along the quasi-equilibrium path, and the images in the lower row are for six points along the non-equilibrium path. It is worth noting that these conformations are constructed from the *expected values* of the system energy and the descriptor parameters, R_g, τ, and R_E along the respective paths. Thus, the conformations shown are not simply instances generated from a single Monte Carlo experiment, but rather, are averaged structures that represent the thermodynamic states along the calculated path. For the quasi-equilibrium path, the initial chain conformation (left-most image) has a well-formed hydrophobic core (the orange spheres represent the hydrophobic monomers) with only a few free monomers apart from the center of mass. The initial state for the non-equilibrium path has a smaller hydrophobic core and segments of non-interacting monomers extending away from the core are more apparent. The two paths have different initial states, but the right-most image on both rows are same because the final stable equilibrium state for quasi-equilibrium and non-equilibrium paths are identical (the same reservoir temperature). Generally speaking, the quasi-equilibrium conformations begin with a relatively compact core that becomes slightly denser as the chain cools to the reservoir temperature, whereas the non-equilibrium path begins with a more open conformation that eventually collapses to the same compact core.

B. Interactions with a High-T Reservoir

To investigate the behavior of the 58-monomer chain during a heating process, the SEAQT equation of motion is solved with a higher reservoir temperature. In this case, heat flows from the reservoir into the polymer until the system equilibrates at the high reservoir temperature. The quasi-equilibrium and non-equilibrium heating paths are shown in Figure 6. Both paths interact with a heat reservoir at a non-dimensional temperature of $k_bT^R/\varepsilon^{\mathrm{HH}} = 1.8$ K. The initial states for the quasi-equilibrium and non-equilibrium heating paths are the same as the initial states employed for the cooling case to the low-temperature reservoir. During heating, the

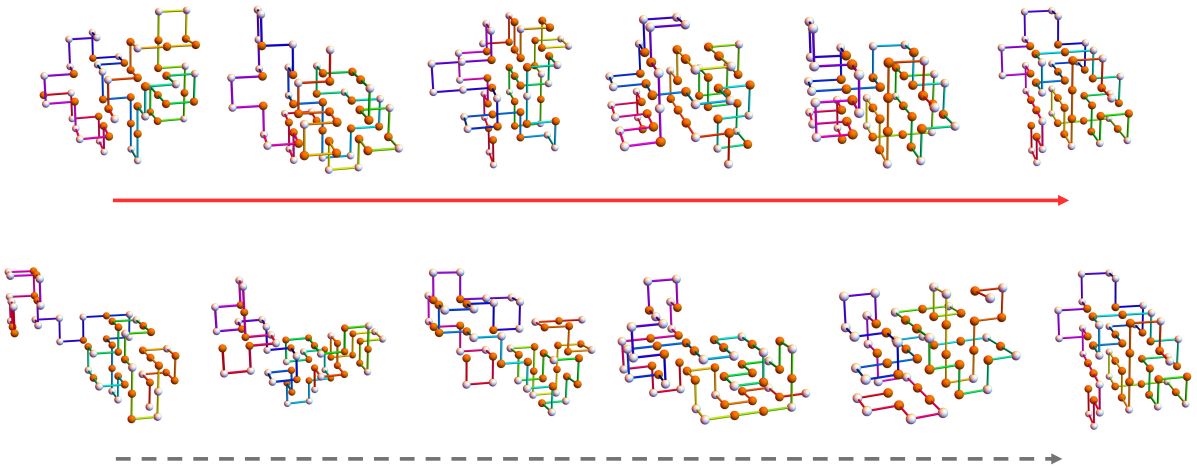


FIG. 5. Polymer chain conformations along the kinetic paths interacting with the low-temperature reservoir are shown in Figure 3. Arrows indicate the direction of evolution from the initial chain conformation (left side) to the stable equilibrium conformation at the reservoir temperature (right side). The solid red arrow represents the sequence of conformations along the quasi-equilibrium path, while the dashed gray arrow corresponds to the sequence along the non-equilibrium path. The stable equilibrium conformation for both paths is identical. The small orange spheres represent hydrophobic monomers and the white spheres represent polar molecules. A color gradient is added to the chain to make the chain's conformation more apparent.

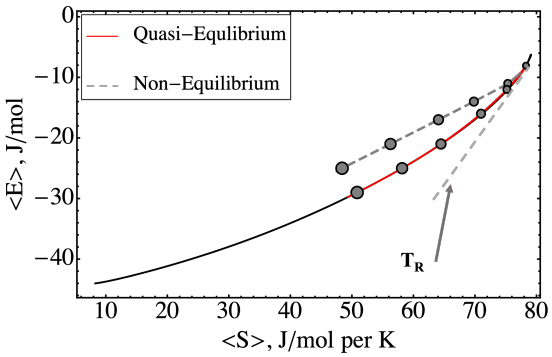


FIG. 6. The SEAQT predicted non-equilibrium path (dashed gray curve) and quasi-equilibrium path (solid red curve) associated with the 58-monomer chain system interacting with a high-temperature reservoir. The dashed light gray line denotes the tangent to the curve of stable equilibrium states (black curve) and is equal to the reservoir temperature. The paths are marked with circles to represent the energy and entropy of the polymer chain conformations shown in Figure 8. The largest circles are the initial states of the two paths, the smallest circle is the final stable equilibrium state at the reservoir temperature.

polymer chain is expected to transition from a globular conformation at its initial state to an uncoiled conformation at the reservoir temperature. Because the degeneracy of the energy levels greatly increases at higher energies (Figure 1), the difference between the quasi- and non-equilibrium paths is also expected to be more pronounced for the heating case.

The evolution of the structural parameters associated with the quasi-equilibrium and non-equilibrium heating paths are shown in Figure 7. The expectation values for the radius of gyration, R_g, and end-to-end distance, R_E, exhibit periods of rapid unfolding for both paths but are much more pronounced for the non-equilibrium path. This is then followed by a gradual increase as the system approaches the equilibrium values. The tortuosity, τ, follows behavior similar to that of R_g and R_E with the primary difference being that the slope for the τ paths is negative. For all three parameters, the change along the non-equilibrium path is initially rapid with a steep slope for a relatively brief amount of time followed by a very gradual increase or decrease to the stable equilibrium value. This contrasts with the quasi-equilibrium path behavior which initially sees a lessened sloped increase or decrease that, however, lasts well along the path before eventually transitioning smoothly to a very gradual asymptotic approach to the stable equilibrium value. The peculiar inflection or initial decrease seen in the tortuosity and the end-to-end distance curves during quasi-equilibrium cooling is not seen in either of the heating paths.

During heating, the energy, and entropy of the polymer increase as heat flows into the system from the reservoir. Consequently, the values of the R_g, τ, and R_E descriptors evolve along heating paths (Figure 7) in opposite directions to the corresponding values along cooling paths (Figure 4).

The expected chain conformations along the non-equilibrium and quasi-equilibrium heating paths of Figure 6 are shown in Figure 8. The chain confirmations

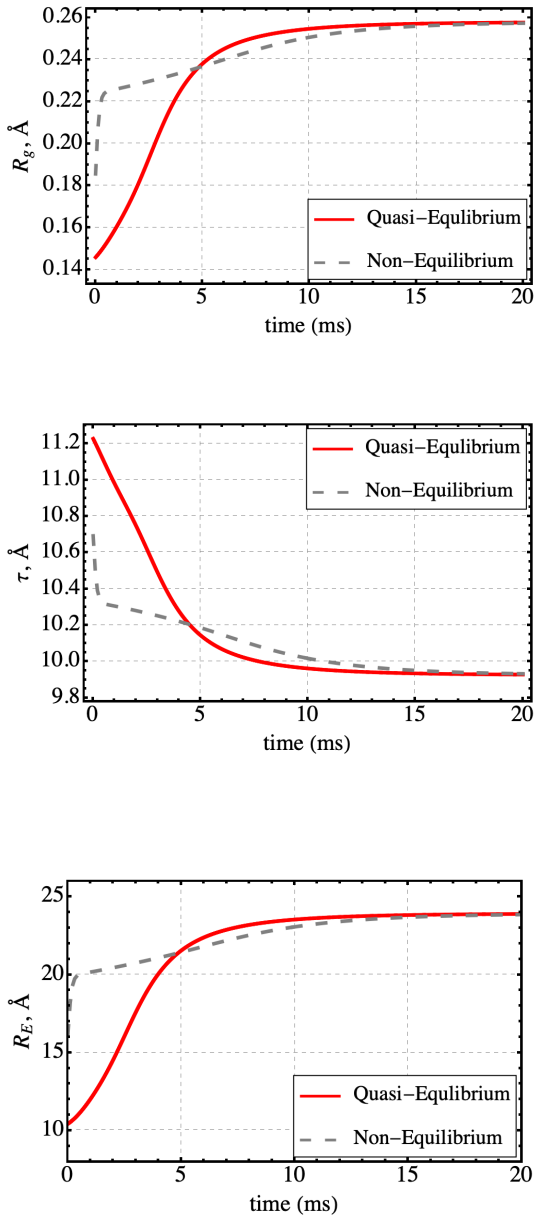


FIG. 7. Evolution of the expectation values of the radius of gyration, the tortuosity, and the end-to-end distance for both the quasi-equilibrium and non-equilibrium paths as the polymer chain interacts with a high-temperature reservoir.

along the quasi-equilibrium path (upper row), and the non-equilibrium path (lower row) begin with a moderately compact hydrophobic core (left most images) and quickly uncoil as heating takes place. As the trends in the descriptor values suggest, the chain conformations in Figure 8 uncoil most quickly along the non-equilibrium path during heating. In addition, the differences between the chain conformations along the quasi-equilibrium and non-equilibrium paths are more apparent during heating (Figure 8) than during cooling (Figure 5).

For both cooling and heating interactions with a thermal reservoir, the expected values of the property descriptors all evolve faster along the non-equilibrium paths than along quasi-equilibrium paths, especially at the initial portion of the kinetic paths. Transitions in chain conformations also are initially more drastic along a non-equilibrium path than along a quasi-equilibrium path [59]

IV. DISCUSSION

A comparison between the predicted results and experimental results found in the literature is very challenging if not impossible. Difficulties arise from the complexity of performing the sensitive experiments and from sequence and monomer length differences between real and simulated systems. Nonetheless, even without such a comparison, polymer folding models can elucidate important information on the nature of the folding of these systems, which can be nearly impossible to analyze experimentally. Thus, though direct comparisons are not possible, our predicted results for the quasi-equilibrium case match the general expectations outlined below, and the non-equilibrium path predictions expand the scope of the studied folding behavior. Polymers have been experimentally verified to form near-native structures, beginning with a rapid collapse occurring over the span of a few to tens of milliseconds. This initial collapse is succeeded by a gradual transition towards the true native structure over hundreds of milliseconds. The rapid collapse and start of the gradual transition are recovered in Figures 4 and 5, which show significant changes in the evolution of the structural properties followed by a period of gradual change as the system approaches stable equilibrium [2, 15, 60–63].

In this work, comparisons are made with the physical kinetics and timescales of sub-millisecond folding results for a 103 monomer protein chain, using relaxation proportionalities taken from Rouse dynamics. In Rouse dynamics [64], the relaxation of a polymer system is related to $\tau = {R_g}^2/D$ where the diffusion coefficient $D \propto 1/N$ and N is the length of the polymer chain. Experimental results show an initial folded collapse of the chain that occurs over a time scale of 0.8 ms for the experimentally researched chain [65]. Though the experimental results are measured using intensity profiles, the rate of change of the generated curves map directly to morphological changes due to the reduced separation of functional groups during initial collapse. The experimental results are most comparable to the radius of gyration since it reflects the significant cluster formation seen in Figure 4, while the tortuosity is expected to gradually increase beyond the initial collapse as the system moves closer to the actual native conformation.

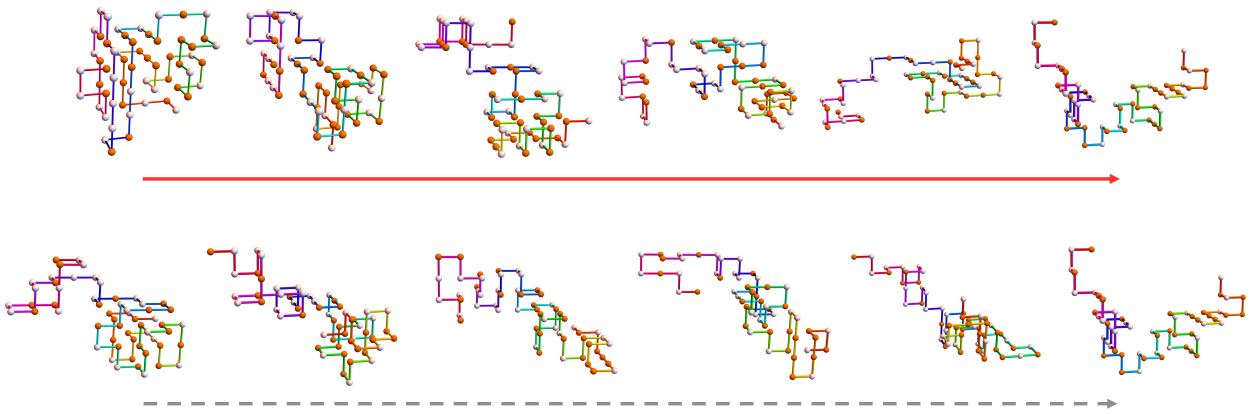


FIG. 8. Polymer chain conformations along the kinetic paths interacting with the high-temperature reservoir are shown in Figure 6. Arrows indicate the direction of evolution from the initial chain conformation (left side) to the stable equilibrium conformation at the reservoir temperature (right side). The solid red arrow represents the sequence of conformations along the quasi-equilibrium path, while the dashed gray arrow corresponds to the sequence along the non-equilibrium path. The stable equilibrium conformation for both paths is identical. The small orange spheres represent hydrophobic monomers and the white spheres represent polar molecules. A color gradient is added to the chain to make the chain's conformation more apparent.

Thus, using the diffusive coefficient to monomer length proportionality, the evolution of the chain studied here can be compared to experimental values by reducing the diffusive evolution by one half to 0.4 ms. Approximate length scales for the polymer chain are made in line with the Lennard-Jones parameter results for the location of the potential well at 4 Å between non-sequenced interacting monomers [66]. This allows accurate scaling of the parameter calculations. The change in the radius of gyration, ΔR_g from the stable equilibrium value for the high-temperature path is ≈ 0.13 Å so that $\Delta R_g^2 = .01$ Å. This value is chosen since the initial image for the low-temperature path representative microstructures, Figure 5, shows evidence of a prior collapse compared to the final image of the high-temperature results, Figure 8. Experimental results for the diffusion coefficient for the protein provide a coefficient of $D = 1 \times 10^{-6}$ cm^2/s. This gives a proportionality constant of $\approx 2.35 \times 10^7$. The potential mutability of this factor can depend on temperature and the modeled system environment, including the available degrees of freedom [10, 11, 60, 62]. However, the value does provide an approximate constant for scaling the magnitude of the results.

Additionally, under high-temperature conditions or denaturing of the chain, the chain is expected to transition through a compact denatured state where the system retains some mass of the hydrophobic core as it uncoils. This behavior is also recovered in our predictions. From Figure 8, the representative chains unravel from the central core, which remains defined, along both paths until the system reaches the highest energy state of the path [15].

Note that the predictions made here are performed without including a specific kinetic folding mechanism and without the risk of the system becoming trapped in local or metastable equilibrium states. The predictions are based only on the energy landscape used and the path predicted by the steepest entropy ascent principle embodied in the SEAQT equation of motion, which drives the system towards mutual stable equilibrium with a chosen low- or high-temperature reservoir.

Finally, the reported results could be used in a variety of ways to optimize statistical searches by formulating reasonable bounds for the chain conformations. In addition, the range of values calculated could be used in Monte Carlo simulations with similar effects to reduce or constrain the search range to a small set of available conformations, potentially improving the computational time by avoiding structures prone to entrapment [2, 15].

V. CONCLUSIONS

Folding transitions of a simple polymer chain are studied using the principle of steepest entropy ascent. In conjunction with a path-independent energy landscape, the steepest entropy ascent principle is employed to describe chain conformations and chain properties along quasi-equilibrium (or near-equilibrium) and non-equilibrium cooling and heating paths. These calculations are performed with no prior assumption of entropy associated with each state or the specific kinetic mechanism governing folding. The Replica Exchange Wang Landau algorithm is utilized to generate the energy landscape, including the necessary degeneracies and the structural parameters associated with each level. The kinetic path through state space is found by solving the SEAQT equation of motion. When applied to a 58-monomer chain with an amino acid sequence taken from Dill *et al.* [16], the following conclusions are drawn:

1. Kinetics predicted by the SEAQT equation of motion agree qualitatively with the radius of gyration and intensity data showing coiling behavior in cytochrome c protein.

2. Simulated folding kinetics can be made physically realistic by fitting the SEAQT relaxation parameter, τ, to experimental kinetics.

3. Representative chain conformations can be constructed from expected values of the system energy and structural descriptors along any kinetic path.

4. SEAQT extends the current application of energy landscapes describing polymer folding by linking a verifiable and thermodynamically bound equation of motion to unique entropy-driven paths through state space.

5. Chain conformations and the properties R_g, τ, and R_E change more drastically along non-equilibrium paths than along quasi-equilibrium paths.

---

* jmcdonald@vt.edu (J. McDonald)
† vonspako@vt.edu (M.R. von Spakovsky)
‡ reynolds@vt.edu (W. T. Reynolds Jr.)

[1] E. I. Shakhnovich, "Theoretical studies of protein-folding thermodynamics and kinetics," *Current Opinion in Structural Biology*, vol. 7, no. 1, pp. 29–40, 1997.

[2] K. A. Dill, "Polymer principles and protein folding (vol 8, pg 1166, 1999)," *Protein Science*, vol. 9, no. 12, pp. 2583–2583, 2000.

[3] K. Yue and K. A. Dill, "Forces of tertiary structural organization in globular-proteins," *Proceedings of the National Academy of Sciences of the United States of America*, vol. 92, no. 1, pp. 146–150, 1995.

[4] T. Wust and D. P. Landau, "Optimized wang-landau sampling of lattice polymers: Ground state search and folding thermodynamics of hp model proteins," *Journal of Chemical Physics*, vol. 137, no. 6, 2012.

[5] A. C. K. Farris, T. Wust, and D. P. Landau, "Statistical physics meets biochemistry: Wang-landau sampling of the hp model of protein folding," *American Journal of Physics*, vol. 87, no. 4, pp. 310–316, 2019.

[6] P. L. Privalov, "Intermediate states in protein folding," *Journal of Molecular Biology*, vol. 258, no. 5, pp. 707–725, 1996.

[7] Z. L. Wang and X. H. He, "Phase transition of a single star polymer: A wang-landau sampling study," *Journal of Chemical Physics*, vol. 135, no. 9, 2011.

[8] G. J. Shi, T. Vogel, T. Wust, Y. W. Li, and D. P. Landau, "Effect of single-site mutations on hydrophobic-polar lattice proteins," *Physical Review E*, vol. 90, no. 3, 2014.

[9] M. Radhakrishna, S. Sharma, and S. K. Kumar, "Enhanced wang landau sampling of adsorbed protein conformations," *Journal of Chemical Physics*, vol. 136, no. 11, 2012.

[10] M. P. Taylor, T. M. Prunty, and C. M. O'Neil, "All-or-none folding of a flexible polymer chain in cylindrical nanoconfinement," *Journal of Chemical Physics*, vol. 152, no. 9, 2020.

[11] M. P. Taylor, C. Vinci, and R. Suzuki, "Effects of macromolecular crowding on the folding of a polymer chain: A wang-landau simulation study," *Journal of Chemical Physics*, vol. 153, no. 17, 2020.

[12] L. S. Ferreira, A. A. Caparica, M. A. Neto, and M. D. Galiceanu, "The rubber band revisited: Wang-landau simulation," *Journal of Statistical Mechanics-Theory and Experiment*, 2012.

[13] A. C. K. Farris, D. T. Seaton, and D. P. Landau, "A first look at lattice effects in coarse-grained protein models via wang-landau simulations," *Xxx Iupap Conference on Computational Physics*, vol. 1290, 2019.

[14] D. T. Seaton, T. Wust, and D. P. Landau, "Collapse transitions in a flexible homopolymer chain: Application of the wang-landau algorithm," *Physical Review E*, vol. 81, no. 1, 2010.

[15] K. A. Dill, S. Bromberg, K. Z. Yue, K. M. Fiebig, D. P. Yee, P. D. Thomas, and H. S. Chan, "Principles of protein-folding - a perspective from simple exact models," *Protein Science*, vol. 4, no. 4, pp. 561–602, 1995.

[16] K. A. Dill, K. M. Fiebig, and H. S. Chan, "Cooperativity in protein-folding kinetics," *Proceedings of the National Academy of Sciences of the United States of America*, vol. 90, no. 5, pp. 1942–1946, 1993.

[17] G. Ping, J. M. Yuan, Z. F. Sun, and Y. Wei, "Studies of effects of macromolecular crowding and confinement on protein folding and protein stability," *Journal of Molecular Recognition*, vol. 17, no. 5, pp. 433–440, 2004.

[18] D. Gersappe, W. X. Li, and A. C. Balazs, "Computational studies of protein adsorption at bilayer interfaces," *Journal of Chemical Physics*, vol. 99, no. 9, pp. 7209–7213, 1993.

[19] V. Castells, S. X. Yang, and P. R. Van Tassel, "Surface-induced conformational changes in lattice model proteins by monte carlo simulation," *Physical Review E*, vol. 65, no. 3, 2002.

[20] T. Cellmer, D. Bratko, J. M. Prausnitz, and H. Blanch, "Protein-folding landscapes in multichain systems," *Proceedings of the National Academy of Sciences of the United States of America*, vol. 102, no. 33, pp. 11692–11697, 2005.

[21] L. Zhang, D. N. Lu, and Z. Liu, "How native proteins aggregate in solution: A dynamic monte carlo simulation," *Biophysical Chemistry*, vol. 133, no. 1-3, pp. 71–80, 2008.

[22] G. C. Li and M. R. von Spakovsky, "Steepest-entropy-ascent quantum thermodynamic modeling of the relaxation process of isolated chemically reactive systems using density of states and the concept of hypoequilibrium state," *Physical Review E*, vol. 93, no. 1, 2016.

[23] G. C. Li and M. R. von Spakovsky, "Generalized thermodynamic relations for a system experiencing heat and mass diffusion in the far-from-equilibrium realm based on steepest entropy ascent," *Physical Review E*, vol. 94, no. 3, 2016.

[24] G. C. Li and M. R. von Spakovsky, "Modeling the nonequilibrium effects in a nonquasi-equilibrium thermodynamic cycle based on steepest entropy ascent and an isothermal-isobaric ensemble," *Energy*, vol. 115, pp. 498–512, 2016.

[25] G. C. Li and M. R. von Spakovsky, "Steepest-entropy-ascent model of mesoscopic quantum systems far from equilibrium along with generalized thermodynamic definitions of measurement and reservoir," *Physical Review E*, vol. 98, no. 4, 2018.

[26] G. Li, M. R. von Spakovsky, and C. Hin, "Steepest entropy ascent quantum thermodynamic model of electron and phonon transport," *Physical Review B*, vol. 97, no. 2, p. 024308, 2018.

[27] G. Li and M. R. von Spakovsky, "Study of Nonequilibrium Size and Concentration Effects on the Heat and Mass Diffusion of Indistinguishable Particles using Steepest-Entropy-Ascent Quantum Thermodynamics," *Journal of Heat Transfer*, vol. 139, no. 12, p. 122003, 2017.

[28] G. Li, M. R. von Spakovsky, F. Shen, and K. Lu, "Multiscale Transient and Steady-State Study of the Influence of Microstructure Degradation and Chromium Oxide Poisoning on Solid Oxide Fuel Cell Cathode Performance," *Journal of Non-Equilibrium Thermodynamics*, vol. 43, no. 1, pp. 21–42, 2018.

[29] J. McDonald, M. R. von Spakovsky, and W. T. Reynolds Jr., "Entropy-driven microstructure evolution calculated with the steepest-entropy-ascent quantum thermodynamic frameworks," *Acta Materialia*, no. accepted, p. http://arxiv.org/abs/2108.11924, 2022.

[30] R. Yamada, M. R. von Spakovsky, and W. T. Reynolds Jr., "A method for predicting non-equilibrium thermal expansion using steepest-entropy-ascent quantum thermodynamics," *Journal of Physics: Condensed Matter*, vol. 30, no. 32, p. 325901, 2018.

[31] R. Yamada, M. R. von Spakovsky, and W. T. Reynolds Jr., "Methodology of an application of the steepest-entropy-ascent quantum thermodynamic framework to physical phenomena in materials science," *Computational Materials Science*, vol. 166, pp. 251–264, 2019.

[32] R. Yamada, M. R. von Spakovsky, and W. T. Reynolds Jr., "Predicting the continuous and discontinuous phase decompositions using the steepest-entropy-ascent quantum thermodynamics modeling," *Phys. Rev. E*, vol. 99, no. 5, p. 052121, 2019.

[33] R. Yamada, M. R. von Spakovsky, and W. T. Reynolds Jr., "Low-temperature atomistic spin relaxation and non-equilibrium intensive properties using steepest-entropy-ascent quantum-inspired thermodynamics modeling," *Journal of Physics: Condensed Matter*, vol. 31, p. 505901, 2019.

[34] R. Yamada, M. R. von Spakovsky, and W. T. Reynolds Jr., "Kinetic pathways of ordering and phase separation using classical solid state models within the steepest-entropy-ascent quantum thermodynamic framework," *Acta Materiala*, vol. 182, pp. 87–99, 2020.

[35] J. A. Montañez Barrera, C. E. Damian-Ascencio, M. R. von Spakovsky, and S. Cano-Andrade, "Steepest-entropy-ascent quantum thermodynamic modeling of decoherence in two different microscopic composite systems," *Physical Review A*, vol. 101, p. 052336, 2020.

[36] S. Cano-Andrade, G. P. Beretta, and M. R. von Spakovsky, "Steepest-entropy-ascent quantum thermodynamic modeling of decoherence in two different microscopic composite systems," *Physical Review A*, vol. 91, no. 1, p. 013848, 2015.

[37] A. Kusaba, G. Li, M. R. von Spakovsky, P. Kempisty, and Y. Kangawa, "Ch_4 adsorption probability on gan(0001) and (000-1) during movpe and its relationship with carbon contamination in the films," *Materials*, vol. 16, no. 6, p. 972, 2019.

[38] A. Kusaba, G. Li, M. R. von Spakovsky, Y. Kangawa, and K. Kakimoto, "Modeling the nonequilibrium process of the chemical adsorption of ammonia on gan(0001) reconstructed surfaces based on steepest-entropy-ascent quantum thermodynamics," *Materials*, vol. 10, no. 8, p. 948, 2017.

[39] M. R. von Spakovsky, C. S. Schlosser, J. B. Martin, and E. Josyula, "Predicting the chemical kinetics of air at high temperatures using steepest-entropy-ascent quantum thermodynamics," in *AIAA 2020 Aviation Forum*, pp. AIAA–2020–3274, American Institute pf Aeronautics and Astronautics, 2020.

[40] G. P. Beretta, "Steepest entropy ascent model for far-nonequilibrium thermodynamics: Unified implementation of the maximum entropy production principle," *Physical Review E*, vol. 90, no. 4, p. 042113, 2014.

[41] G. P. Beretta, "Nonlinear model dynamics for closed-system, constrained, maximal-entropy-generation relaxation by energy redistribution," *Physical Review E*, vol. 73, no. 2, p. 026113, 2006.

[42] G. P. Beretta, E. P. Gyftopoulos, J. L. Park, and G. N. Hatsopoulos, "Quantum thermodynamics - a new equation of motion for a single constituent of matter," *Nuovo Cimento Della Societa Italiana Di Fisica B-General Physics Relativity Astronomy and Mathematical Physics and Methods*, vol. 82, no. 2, pp. 169–191, 1984.

[43] G. P. Beretta, E. P. Gyftopoulos, and J. L. Park, "Quantum thermodynamics - a new equation of motion for a general quantum system," *Nuovo Cimento Della Societa Italiana Di Fisica B-General Physics Relativity Astronomy and Mathematical Physics and Methods*, vol. 87, no. 1, pp. 77–97, 1985.

[44] G. N. Hatsopoulos and E. P. Gyftopoulos, "A unified quantum theory of mechanics and thermodynamics. Part I. postulates," *Foundations of Physics*, vol. 6, no. 1, pp. 15–31, 1976.

[45] G. N. Hatsopoulos and E. P. Gyftopoulos, "A unified quantum theory of mechanics and thermodynamics. Part IIa. Available energy," *Foundations of Physics*, vol. 6, no. 2, pp. 127–141, 1976.

[46] G. N. Hatsopoulos and E. P. Gyftopoulos, "A unified quantum theory of mechanics and thermodynamics. Part IIb. Stable equilibrium states," *Foundations of Physics*, vol. 6, no. 4, pp. 439–455, 1976.

[47] G. N. Hatsopoulos and E. P. Gyftopoulos, "A unified quantum theory of mechanics and thermodynamics. Part III. Irreducible quantal dispersions," *Foundations of Physics*, vol. 6, no. 5, pp. 561–570, 1976.

[48] G. P. Beretta, "The fourth law of thermodynamics: steepest entropy ascent," *Philosophical Transactions of the Royal Society A*, vol. 378, no. 2170, p. 20190168, 2020.

[49] K. F. Lau and K. A. Dill, "A lattice statistical-mechanics model of the conformational and sequence-spaces of proteins," *Macromolecules*, vol. 22, no. 10, pp. 3986–3997, 1989.

[50] J. M. Deutsch, "Long range moves for high density polymer simulations," *Journal of Chemical Physics*, vol. 106, no. 21, pp. 8849–8854, 1997.

[51] M. Bachmann and W. Janke, "Density of states for hp lattice proteins," *Acta Physica Polonica B*, vol. 34, no. 10, pp. 4689–4697, 2003.

[52] T. Vogel, Y. W. Li, T. Wust, and D. P. Landau, "Generic, hierarchical framework for massively parallel wang-landau sampling," *Physical Review Letters*, vol. 110, no. 21, 2013.

[53] T. Vogel, Y. W. Li, T. Wust, and D. P. Landau, "Scalable replica-exchange framework for wang-landau sampling," *Physical Review E*, vol. 90, no. 2, 2014.

[54] T. Vogel, Y. W. Li, T. Wust, and D. P. Landau, "Exploring new frontiers in statistical physics with a new, parallel wang-landau framework," *Vii Brazilian Meeting on Simulational Physics*, vol. 487, 2014.

[55] Y. W. Li, T. Vogel, T. Wuest, and D. P. Landau, "A new paradigm for petascale monte carlo simulation: Replica exchange wang-landau sampling," *25th Iupap Conference on Computational Physics (Ccp2013)*, vol. 510, 2014.

[56] G. P. Beretta, "Nonlinear quantum evolution equations to model irreversible adiabatic relaxation with maximal entropy production and other nonunitary processes," *Reports on Mathematical Physics*, vol. 64, no. 1-2, pp. 139–168, 2009.

[57] E. P. Gyftopoulos and E. Cubukcu, "Entropy: Thermodynamic definition and quantum expression," *Physical Review E*, vol. 55, no. 4, pp. 3851–3858, 1997.

[58] I. Carmesin and K. Kremer, "The bond fluctuation method - a new effective algorithm for the dynamics of polymers in all spatial dimensions," *Macromolecules*, vol. 21, no. 9, pp. 2819–2823, 1988.

[59] "Faster" or "more drastic" here refers to the change in a property with an incremental change along the kinetic path in state space. This is not the same as the time rate with which the kinetic path is traversed.

[60] C. K. Chan, Y. Hu, S. Takahashi, D. L. Rousseau, W. A. Eaton, and J. Hofrichter, "Submillisecond protein folding kinetics studied by ultrarapid mixing," *Proceedings of the National Academy of Sciences of the United States of America*, vol. 94, no. 5, pp. 1779–1784, 1997.

[61] W. A. Eaton, "Modern kinetics and mechanism of protein folding: A retrospective," *Journal of Physical Chemistry B*, vol. 125, no. 14, pp. 3452–3467, 2021.

[62] D. Thirumalai and S. A. Woodson, "Kinetics of folding of proteins and rna," *Accounts of Chemical Research*, vol. 29, no. 9, pp. 433–439, 1996.

[63] K. A. Dill, S. B. Ozkan, M. S. Shell, and T. R. Weikl, "The protein folding problem," *Annual Review of Biophysics*, vol. 37, pp. 289–316, 2008.

[64] P. E. Rouse, "A theory of the linear viscoelastic properties of dilute solutions of coiling polymers," *Journal of Chemical Physics*, vol. 21, p. 1272, 1953.

[65] K. Binder, P. Y. Lai, and J. Wittmer, "Monte-carlo simulations of chain dynamics in polymer brushes," *Faraday Discussions*, vol. 98, pp. 97–109, 1994.

[66] G. Rossi, L. Monticelli, S. R. Puisto, I. Vattulainen, and T. Ala-Nissila, "Coarse-graining polymers with the martini force-field: polystyrene as a benchmark case," *Soft Matter*, vol. 7, no. 2, pp. 698–708, 2011.